

SOIL SALINIZATION DUE TO SALTWATER INTRUSION IN COASTAL REGIONS: THE ROLE OF SOIL CHARACTERISTICS AND HETEROGENEITY

Vahid Sobhi Gollo¹ , Muhammad Sahimi² , Eva González³ ,
Mithra-Christin Hajati³ , Jörg Elbracht³ , Peter Fröhle⁴ , Nima Shokri¹ 

¹Institute of Geo-Hydroinformatics, Hamburg University of Technology, Hamburg, Germany; ²Mork Family Department of Chemical Engineering and Materials Science, University of Southern California, Los Angeles, CA, USA; ³Geological Survey of Lower-Saxony, Hannover, Germany; ⁴Institute of River and Coastal Engineering, Hamburg University of Technology, Hamburg, Germany

Correspondence to:

Vahid Sobhi Gollo:
vahid.sobhi.gollo@tuhh.de

or

Nima Shokri:
nima.shokri@tuhh.de

Institute of Geo-Hydroinformatics,
Hamburg University of Technology, 21073
Hamburg, Germany
Tel: +49 40 42878 2870

How to Cite:

Sobhi Gollo, V., Sahimi, M., González, E., Hajati, M.-C., Elbracht, J., Fröhle, P., & Shokri, N. (2024).

Soil salinization due to saltwater intrusion in coastal regions: The role of soil characteristics and heterogeneity. *InterPore Journal*, 1(1), ipj260424–6.

<https://doi.org/10.69631/ipj.v1i1nr15>

RECEIVED: 22 Nov. 2023

ACCEPTED: 15 Mar. 2024

PUBLISHED: 26 Apr. 2024

ABSTRACT

Soil plays a vital role in maintaining ecosystem functionality, supporting biodiversity, facilitating successful crop production, and ensuring socio-economic stability. Soil quality is, however, constantly threatened by various factors, such as adverse climate conditions, hydrogeological processes, and human activities. One particularly significant stressor is soil salinity, which has a detrimental effect on soil quality. This study focuses specifically on understanding how soil properties contribute to the accumulation of surface soil salinity in the presence of shallow saline groundwater. To achieve this objective, advanced groundwater modeling techniques are employed to simulate saltwater intrusion in a riparian area known as Altes Land in northern Germany. A realistic representation of the salinization process is created and evaluated using a comprehensive dataset of hydrogeological information specific to the region. Additionally, the study examines the influence of soil heterogeneity on regional soil salinity by varying soil properties through devising six distinct scenarios for generating the numerical models that represent variations in soil texture and structure. The study reveals that regional soil texture and layering arrangement significantly influence the availability of water and the propagation of saline water in the vadose zone, and are major contributors to surface soil salinity. Subtle alterations and simplifications, often inconspicuous or deemed inconsequential in the context of small-scale experiments, may carry substantial ramifications for the formulation of enhanced management strategies in regions characterized by low elevation and influenced by groundwater salinity. Furthermore, the insights gained from this research provide valuable information for applications in agricultural practices and environmental conservation.

Plain language summary

Saltwater intrusion occurs when seawater enters coastal groundwater. In low-lying coastal regions, saline groundwater can rise close to the soil surface, leading to soil salinization that negatively impacts soil health and plant growth. The extent of soil salinization can be impacted by soil texture and heterogeneity, which is not fully understood at regional scales. In this study, we developed a new decision-support framework capable of describing and predicting salt transport through unsaturated zones lying over groundwater affected by seawater intrusion, and evaluated it

against field measurements. This enabled us to investigate soil salinity under a variety of conditions and quantify the effects of important parameters, including soil texture, heterogeneity, and layering arrangement, on salt deposition close to the surface. Our study offers new quantitative insights into and tools for revealing the mechanisms governing the spatial distribution of soil salinity, as well as its health, hence contributing to global efforts for sustainable resource management and United Nations Sustainable Development Goals, particularly UN SDG15.

KEYWORDS

Soil salinity, Seawater intrusion, Soil characteristics, Soil health, Soil remediation



@2024 The Authors

This is an open access article published by InterPore under the terms of the Creative Commons Attribution-NonCommercial-NoDerivatives 4.0 International License (CC BY-NC-ND 4.0) (<https://creativecommons.org/licenses/by-nc-nd/4.0/>).

1. INTRODUCTION

Healthy soil is essential for ecosystem functioning and services, biodiversity, crop production, and socioeconomic stability. Adverse regional climate conditions, such as drought stress, heat waves, high temperatures, and flooding, in conjunction with challenging soil conditions, such as nutrient deficiency, soil salinity, and extreme pH, along with the presence of ubiquitous pollutants, such as heavy metals, microplastics, herbicides, pesticides, antibiotics, and organic pollutants, can potentially reduce soil quality significantly and endanger major crops, global food production, and food security (14, 59, 66, 84). Many studies have extensively examined the influence of various stressors on crop responses, including high temperatures (3, 6), soil salinity (38, 58), heavy metals (4), and microplastics (57).

There currently exists a substantial body of published research dedicated to examining the sources of soil quality stressors (e.g. 18, 50). Several studies have extensively examined the role of climate (29, 48, 49), human activities (32, 78, 85, 87), and the hydrogeological features of landscapes (40, 82) to assess their impact on soil quality. Climate factors exhibit a direct correlation with stressors such as drought and high temperatures and exert a regulatory influence on soil contamination. Human activities such as irrigation have also been identified as potential contributors to alterations in soil salinity (43). Furthermore, the introduction of pesticides and fertilizers, as well as the influx of urban and industrial effluents, has the inherent capability to disturb soil chemistry and elevate the concentrations of pollutants (86). Moreover, hydrogeological conditions, including soil morphology and chemical composition (1, 19, 52), groundwater hydraulic conditions (8, 21), and terrain properties, such as slope (30, 44), can potentially affect soil quality.

As described above, various climatic, anthropogenic, and hydrogeological factors can potentially contribute to the escalation of soil salinity levels, which in turn can lead to the depletion of fertile agricultural soil, posing a significant threat to food security. Our research focuses on advancing the understanding of the hydrogeological factors involved in the development of soil salinity. Specifically, we aimed to further explore the relationship between soil properties and the upward transport of saline water to the surface, which occurs in the presence of shallow saline groundwater that is hydraulically connected to the soil surface through the vadose zone (28, 35, 61, 72). Extensive investigation of this process has been carried out using various techniques across many spatial scales. Using stochastic modeling techniques, Shah et al. (67) carried out a study to examine the accumulation of salt in the root zone that results from capillary flux from brackish groundwater, while also accounting for the osmotic effects of the dissolved salt mass. Their findings indicated that the salinity of the root zone exhibited an almost linear relationship with the groundwater salinity. Narjary et al. (45) employed a one-dimensional (1D) groundwater model to investigate the influence of the depth of shallow saline groundwater table on dynamics of soil salinity. Their research revealed that as the depth of the saline groundwater table increased, there was an increase in upward salt movement, leading to elevated soil salinity levels.

Li and Shi (37) focused on the impact of salt precipitation growth on upward solute transport and the spatial distribution of temperature in sandy soils with a fixed depth of groundwater table. Their investigation indicated that the lateral growth of salt precipitation has a minimal effect on the transport process, whereas the elevated salt crust substantially reduces the transport rates and lowers soil profile temperatures due to increased albedo and the formation of an air layer. Norouzi Rad et al. (47, 51) studied salt precipitation in drying porous media in order to understand the complex dynamics and the patterns of salt deposition. One study (47) focused on the pore-scale dynamics of salt precipitation using high-resolution X-ray microtomography and scanning electron microscopy, revealing non-uniform salt precipitation patterns in porous media, which are influenced by the spatial distribution of the pore sizes. In the second study (51), X-ray micro-tomography was used to investigate the effect of particle and pore sizes on salt precipitation patterns and dynamics, and it was reported that preferential upward transport sites, associated with fine pores, significantly influence the patterns and dynamics of NaCl precipitation on the surface of sand columns.

Hassani et al. (23) proposed a machine-learning approach to predict soil salinity and sodicity at a global scale over the past four decades. Their analysis revealed that a substantial portion of non-frigid regions, particularly in Asia (China, Kazakhstan, and Iran), Africa, and Australia, was affected by salt, with frequent recurrence between 1980 and 2018. In another study (24) they investigated the impact of climate change on naturally occurring soil salinization in global drylands by developing data-driven models to predict primary soil salinity and its variations up to the year 2100. Their study identified future salinization hotspots worldwide.

In a laboratory experiment utilizing alternating layers of coarse and fine sand, Shokri et al. (70) demonstrated that textural interfaces have a strong impact on the capillary rise phenomenon. This has implications and significance in soil on a large scale, because soil and other natural porous media are typically stratified. Shokri (68) employed synchrotron X-ray micro-tomography to investigate water transport from saline porous media. The results indicate that, consistent with the theory of wetting in porous media (63), air (a non-wetting fluid) invades large pores at the surface, whereas finer pores remain connected to the wet zone at the bottom, leading to higher salt concentrations in the finer pores. Dashtian et al. (9) utilized a pore-network model to investigate salt transport and precipitation in porous media. Their work emphasized the significance of pore space morphology and the clustering of areas in which salt precipitation has occurred, especially in natural porous media that typically contain stratification.

Soil layering and sharp vertical textural contrasts are common in coastal environments (27, 83). Recent advancements, such as those mentioned above, have led to significant progress in understanding the relationship between soil properties, such as soil type, stratification, and sharp soil textural contrasts, their impact on the vertical transport of saline water, and the subsequent increase in soil salinity (36). It is now possible to accurately estimate the upward movement of saline water in a pore/laboratory/field-scale soil column (73), evaluate the effect of various types of soil stratifications on the extent of upward transport of saline water (7), and develop an approximate mapping of how soils with various compositions contribute to soil salinity on a global scale (23, 24). For instance, it is well known that when the top layer of soil is sandy, which means it has larger particles and can hold less water, water does not move easily through it and does not reach the surface as much as it would in soil with smaller particles, such as silt (63). Moreover, in heterogeneous soil, sandy soil on top of silt soil can block the upward flow of water, preventing it from reaching the surface (70).

However, when considering practical applications in agricultural regions affected by salinity in shallow regional groundwater, such as those that experience saltwater intrusion, there remains a lack of comprehensive understanding of the extent of the influence of soil properties and textural variations on the development of soil salinity resulting from interaction with groundwater. Several assumptions, such as the imposition of soil homogeneity through the application of effective hydraulic conductivity to the entire laboratory sample, or the subdivision of the soil sample into homogenous parts with an assumption of homogeneity for each segment, pose challenges in terms of upscaling to a practical

regional scale. Small-scale approaches overlook the impact of minimal and often imperceptible changes in soil texture on the surface, changes that could become especially pronounced when extrapolating results to a practical regional scale. This becomes particularly problematic in the context of investigating the influence of saline groundwater on soil surface salinity at a regional scale, rendering existing experimental results inadequate for a comprehensive assessment of these processes in a larger geographical context. Although phenomena such as saltwater intrusion, which refers to the movement of saline water into freshwater aquifers or surface water bodies, have been extensively studied (20, 60, 79), the influence of soil heterogeneity on the response of regional soil salinity to saltwater intrusion has not been adequately addressed.

Motivated by this knowledge gap, our study aims to develop a robust numerical framework designed to capture the influence of soil heterogeneity on regional soil heterogeneity in the presence of shallow saline groundwater. To achieve our objective, we employed advanced groundwater modeling techniques to simulate saltwater intrusion in a near-coastal riparian area known as Altes Land (see below). Due to its characteristics, this region serves as an ideal study area, as it is a relatively flat terrain with shallow saline groundwater, and is recognized as a significant agricultural hotspot.

By utilizing numerical simulations, we aimed to realistically represent the salinization process in the study area. The model was then evaluated against a substantial dataset of hydrogeological information available for the region, which provides valuable insights into the behavior of shallow salinized groundwater, enabling a more accurate description of the optimal model characteristics. To model saltwater intrusion into the groundwater, we used FEFLOW (11), a groundwater modelling software capable of modelling realistic hydraulic conditions as well as solute (saline water) transport under relatively saturated conditions. After evaluating the model against the available data for saltwater intrusion, we proceed to vary the soil properties of the uppermost layer in the model in order to generate six distinct models -hereafter referred to as scenarios – which represent variations in soil texture and structure. Subsequently, we analyzed the resulting soil salinities for each model within a comprehensive framework to elucidate the impact of contrasting soil textures and structures at a regional scale. We show that by employing a systematic approach to analyze and comprehend the influence of regional soil texture and structure on soil salinity, our work and results provide valuable insights that contribute to refining management strategies aimed at effectively alleviating the complications arising from salinity in low-lying regions impacted by groundwater. The significance of our findings transcends theoretical implications confined to pore/laboratory-scale experiments or rough global estimations, as they hold substantial potential for practical applications in the domains of agricultural practices and environmental conservation.

2. MATERIALS AND METHODS

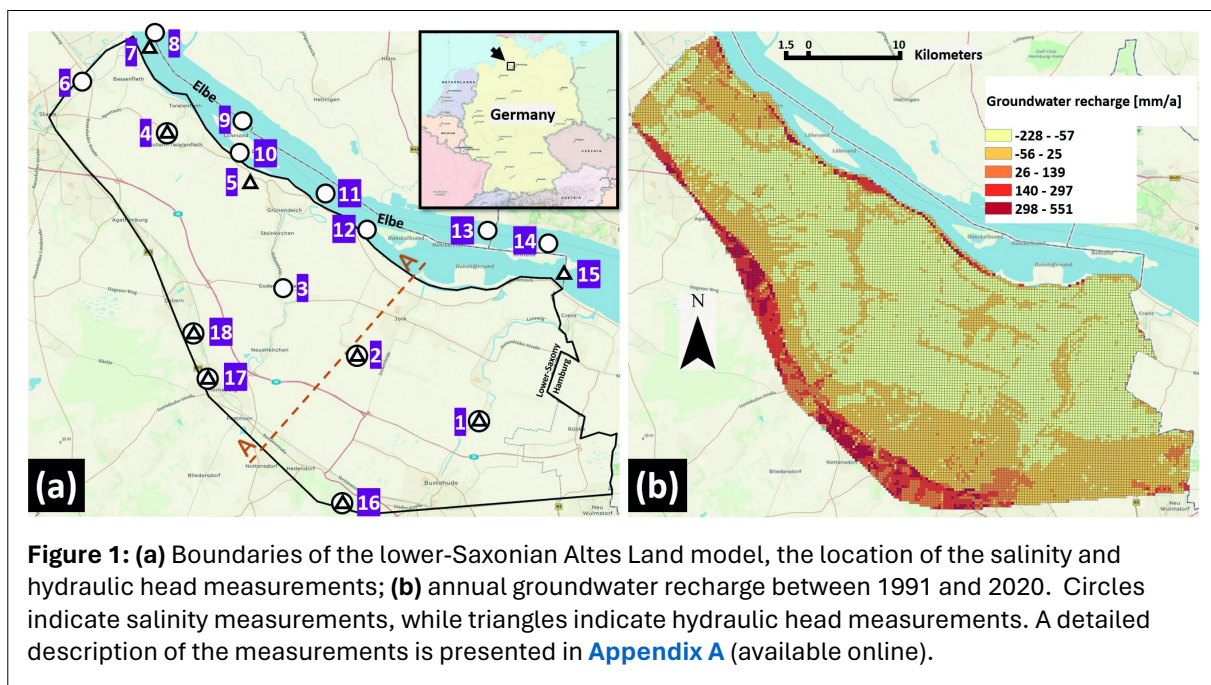
2.1. Study area

As shown in [Figure 1](#), we used a part of Altes Land as the study area for model evaluation and further assessment. Altes Land is characterized by flat, dike-protected land dominated by orchards near the Elbe River in northern Germany (5). The region is a popular cultural attraction and the largest contiguous fruit-producing region in Central Europe. Fruit production in Altes Land is dominated by apples, plums, and cherries (34). The region's apple plantations account for approximately 90% of the acreage, producing approximately 340,000 tons of apples annually (10). However, because of its proximity to the Elbe River, high salinity is a major issue for irrigation and crop production.

2.2. Initial and boundary conditions

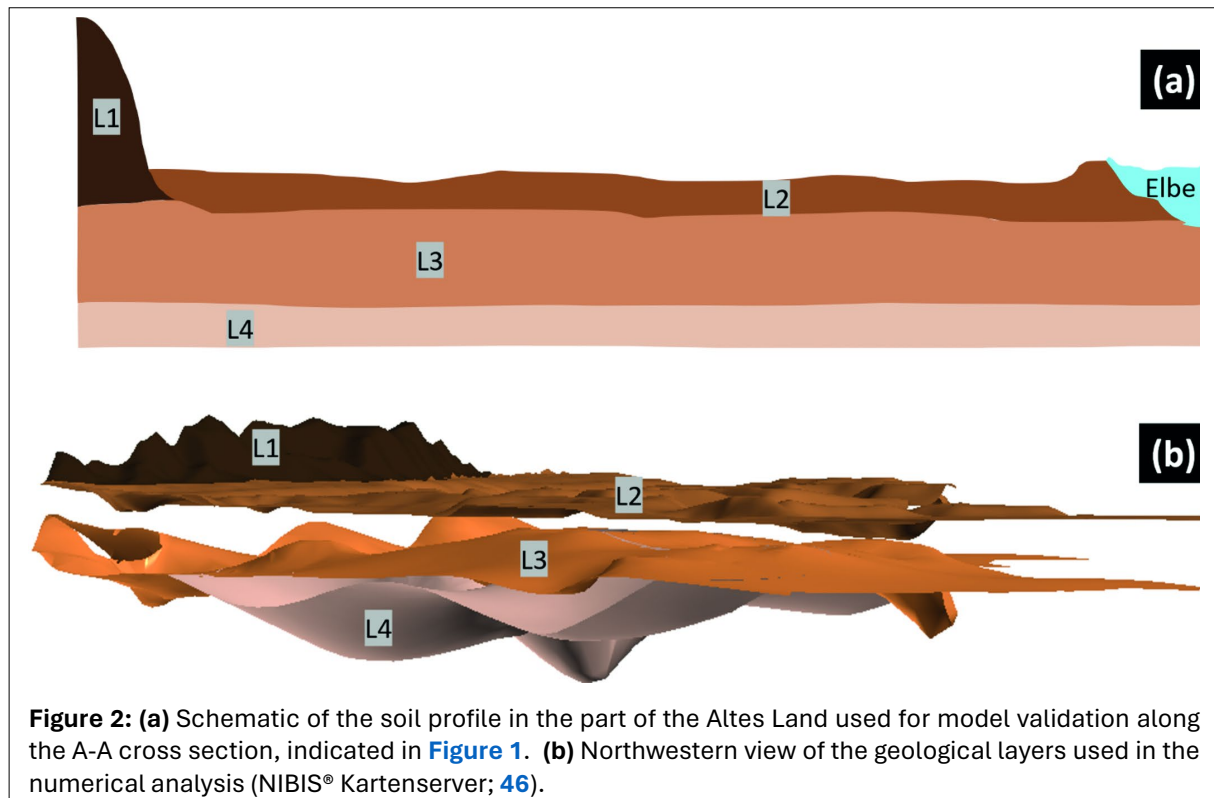
The Lower Saxonian part of the Altes Land (most of the region) was selected as the study domain because of the availability of the data and accessibility. The boundaries of the model are shown in **Figure 1** (see **Appendix A**, available online, for complete information). To the north, the boundaries are defined by the Elbe River. Tidal effects strongly influence this part of the river, resulting in transport of saline water from the North Sea to the river. **Figure 1** presents the location of groundwater, surface water levels, and salinity data, as well as the annual mean groundwater recharge model provided by the Geological Survey of Lower Saxony (GSLs). The groundwater salinity data used in this study were measured from the samples taken directly from each measurement location (74).

The annual average groundwater recharge (**Fig. 1b**) was simulated using the conceptual distributed hydrological water balance model, mGROWA (13, 26). mGROWA relies on various inputs, including precipitation, evaporation, soil characteristics, and landscape features, to estimate annual mean groundwater recharge. In its latest iteration, mGROWA22, groundwater recharge is computed by incorporating precipitation data adjusted using the Richter method (54, 56) and potential evaporation



data calculated using the FAO method from the German Weather Service (DWD). Soil property information sourced from the soil map BK50 (16) is utilized within mGROWA22. The model resolves the daily soil water balance across five soil layers, subsequently partitioning monthly seepage into its constituent discharge components, including groundwater recharge and direct discharge, encompassing drainage, interflow, and surface runoff.

Initially, the model soil was assumed to be fully saturated. In the numerical simulation, we defined the hydraulic head and salinity boundaries along the Elbe River by utilizing the mean salinity of the water levels. Specifically, using the rich historical data available in this study, we employed the mean water levels obtained at points 7 and 15 of **Figure 1** for hydraulic heads (average of daily measurements spanning from 1997 to 2010) and at points 8-14 for salinity (average of weekly measurements spanning at least from 2010 to 2020; for more information, see **Appendix A** online). Using linear interpolation between these points, we determined the hydraulic heads and salinities of all the boundary nodes along



the river. To establish the landward boundaries, we employed the same methodology. We chose measurements at specific locations, namely, points 7, 15-18, to set hydraulic head boundaries, and at points 6, 14, 16-18 to set salinity boundaries. The time span and frequency of the measurements at each sampling location and the average values are available in Appendix A. In the Altes Land region, the annual changes in the groundwater table and salinity were negligible. Therefore, in our model evaluations we used the mean values over the entire measurement period. Note that in the events of precipitation, base flow, or runoff, some areas in the model may have hydraulic heads that are greater than the elevation of the area. To avoid such unrealistic hydraulic heads in the simulations, the maximum hydraulic head was defined to be equal to the point elevation, and excess water was removed from the system. In Altes Land, excess water can theoretically be drained because of the intricate connection of orchards via a dense network of canals. These canals play a pivotal role in both the distribution of water and alleviation of excess water from saturated soil. This drainage system was thoroughly incorporated into the ground-water recharge model, effectively preempting the impact of sporadic hydraulic head surges.

Figure 2 depicts cross-sectional (A-A in Fig. 1) and side views of the geological layers of Altes Land. In coastal areas of northern Europe, moorlands, such as Altes Land, form between the sea (or the river in the case of Altes Land) and sandy hills, as shown in Figure 2 (denoted by L1). In the Holocene transgression phase, before the human-made dikes were built to reclaim the land, these areas were covered with water, resulting in deposition of a silty clayey and partially fine sandy layer (31). This geological layer is currently found across northern German coastal areas with an average thickness of 25 m. Its thickness in Altes Land (Fig. 2, L2) is limited to approximately 12 meters. Prior to the formation of this layer, during the Saalian glaciation period, a sandy glaciofluvial layer formed in marshes and moorlands. This layer in Altes Land (Fig. 2, L3) is approximately 40 m deep on average. Below this layer, a clayey layer formed in glacial reservoirs upstream of the north German glaciers during the melting ice phase (75). Layer L4, shown in Figure 2, with an average thickness of about 25 m and a hydraulic conductivity of about 10⁻⁹ m/s, was selected as the bottom of the aquifer (42).

Since the soil data provided by the geological survey of Lower-Saxony were characterized by German standards of soil characterization, we defined the soil characteristics of each layer according to DIN 4220 (German soil characterization standard; 12), with their van Genuchten parameters (76) displayed in **Table 1**. The properties of each soil layer were used in the simulations. The model was discretized into 250,000 prismatic elements consisting of 47 vertical layers. We constructed the topology of the top layer using the MERIT DEM database (81), with a spatial resolution of 250 m.

Table 1: DIN 4220-compliant soil parameters for the study area.

Layer name	Textural class	θ_r [m ³ /m ³]	θ_s [m ³ /m ³]	α [1/m]	n	kf [m/d]
L1	Sand*	0	0.39	26.4	1.35	3.75
L2	Moderate clayey silt	0.005	0.4	1.7	1.21	0.41
L3	Coarse sand	0	0.38	22.1	1.47	20.99
-	Silt*	0	0.4	1.4	1.21	0.32

*Displayed in **Figure 6** for soil texture scenarios.

Salinity levels in groundwater can influence fluid characteristics, including viscosity and density (15, 65). However, due to the minimal impact on viscosity, we deemed the variability in salinity-induced impacts on the hydraulic conductivity of sand and silt insignificant. Conversely, to comprehensively integrate salinity-induced changes in fluid density into our analyses, we employed density-dependent flow simulations. In this method, the hydraulic heads defined for the boundaries are influenced by the vertical distribution of fluid with varying salinities, resulting in a higher hydraulic head for a point at the same elevation in more saline water compared to less saline water.

2.3. The governing equations and modelling approach

Unsaturated flow through porous media is simulated using Richard's equation (Eq. 1), given by (55) where θ [m³/m³] is the volumetric water content, h [m] is the head induced by capillary action, t [s] is the time, K [m/s] is the hydraulic conductivity, and H [m] is the hydraulic head.

$$\frac{\partial \theta}{\partial t} = \nabla \cdot [K(h)\nabla H] \quad (1)$$

We used the FEFLOW software to numerically solve Richard's equation in a 3D domain. To simulate mass transport, the hydrodynamic dispersion equation was solved numerically under the steady-state assumption (Eq. 2) where v [m/s] is the velocity field, C [g/l] is the solute concentration, D [m] is the dispersion coefficient tensor, and R [g/l] is the sink/source term.

$$v \cdot \nabla C - \nabla \cdot (D\nabla C) = R \quad (2)$$

In consideration of the scale of our numerical domain, we established the longitudinal and transversal dispersivity ranges by adopting the methodologies outlined by Gelhar and Collins (17). Through the execution of a sensitivity analysis correlating mesh resolution with dispersion, we determined a longitudinal dispersion value of 1×10^3 m. Assuming transversal dispersion to be one-tenth of the longitudinal dispersion, we established a transversal dispersion value of 1×10^2 m. By refining the mesh accordingly, we achieved a maximum Péclet number < 0.5 to ensure that diffusive transport is dominant, as expected in groundwater (33).

The model operates under density-dependent flow conditions. Nevertheless, as the ensuing results elucidate, the negligible disparity in salt concentrations within the model, ranging from 237 to 725 mg/l, led to closely aligned densities. Consequently, the detection of saltwater intrusion toe is imperceptible.

3. RESULTS

3.1. Model evaluation

The simulated steady-state hydraulic head, salt concentration, and water content in Altes Land are presented in **Figure 3**, along with the calculated surface soil salinity across the soil surface. In order to calculate the amount of salt deposited on the surface, we used **Equation 3** where $M_s \left[kg \cdot \frac{m^3}{m^3} \right]$ is the

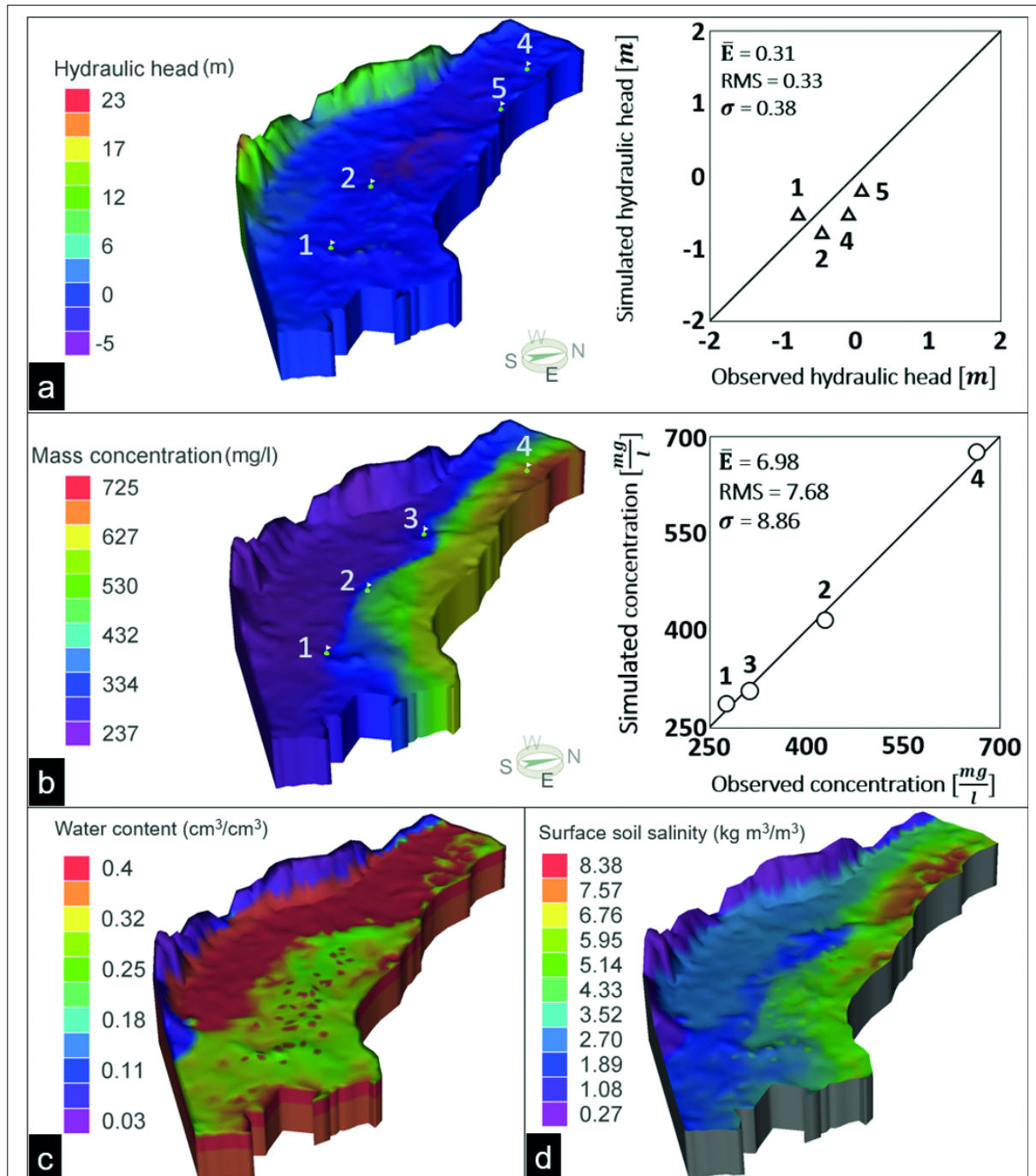


Figure 3: Simulated (a) hydraulic head, and (b) groundwater salt concentration distribution across the Altes Land region, and their comparison with the data at the observation points 1-5. (c) The computed distribution of water content. (d) Calculated surface soil salinity from (b) and (c) using **Equation 3** with an area (A) = 102 m² and soil depth (d) = 0.3 m, where \bar{E} = absolute error, RMS = root mean square, and σ = the standard deviation.

mass of deposited salt over the surface area $A[m^2]$ with a depth of $d[m]$ (root zone), and $\bar{\theta} \left[\frac{cm^3}{cm^3} \right]$ and $\bar{C} \left[\frac{kg}{m^3} \right]$ are, respectively, the mean water content and mean salt concentration in the root zone.

$$M_s = A \cdot d \cdot \bar{\theta} \cdot \bar{C} \quad (3)$$

Based on a global study by Schenk and Jackson (64), 90% of soil profiles have at least 50% of roots in the top 0.3 m of the profile. Therefore, we used $d = 0.3$ m in order to calculate the deposited salt close to the surface.

Before studying soil salinity in the region, we evaluated the simulation results by comparing the computed hydraulic heads (Fig. 3a) and groundwater salt concentrations (Fig. 3b) to the measurements. The simulated mass concentrations corresponding to depths identical to the measured groundwater salinities were employed in this evaluation. As shown in Figure 3, four observation points can be used to evaluate the simulated hydraulic conditions and salt transport. Given the size of the domain considered, there is reasonable agreement between the simulation results and data at the observation points, validating our approach and the model.

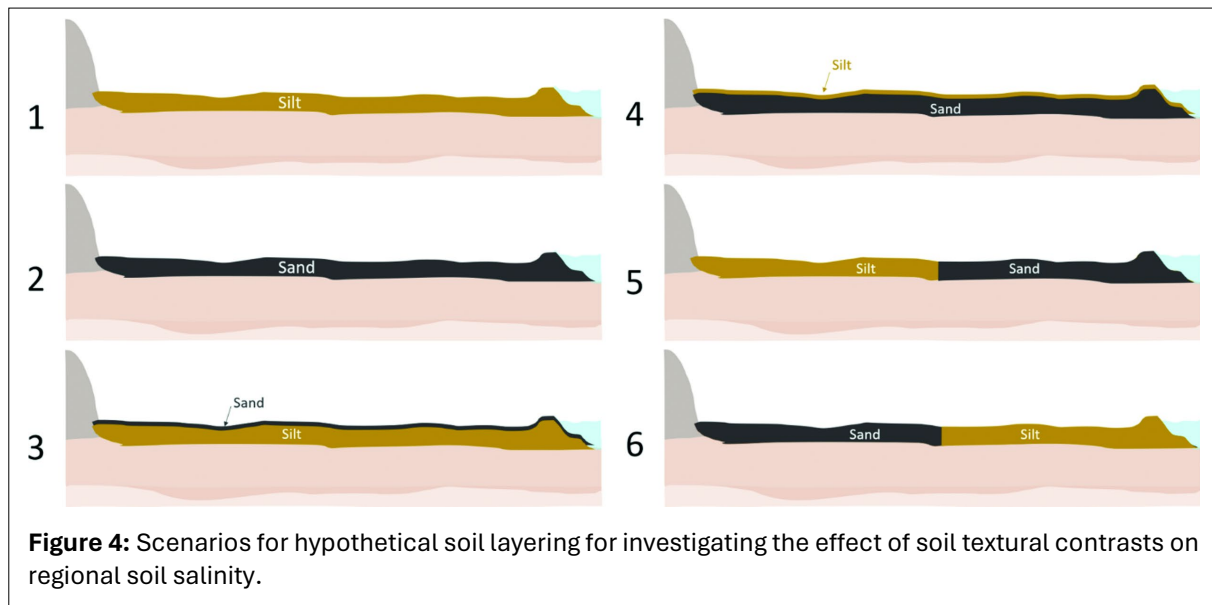
Figure 3b illustrates the gradient of groundwater salt concentration from the river to the land, with the highest salinity in the northwest region (downstream of the river). These areas, located closer to the mouth of the Elbe River, are significantly influenced by the North Sea, resulting in higher salinity levels. As previously mentioned, apple and plum trees, which are highly sensitive to salinity, play a crucial role in the agricultural industry of Altes Land. A salinity level between 640 and 960 mg/l represents a threshold for root water uptake at and above which yields begin to decline (39). Given that the simulated salinities shown in Figure 3 are the mean values, agricultural regions in Altes Land, particularly those adjacent to the Elbe River, may already be at risk of being strongly impacted by soil salinity.

Figure 3d shows the calculated soil salinity of the region's surface using Equation 3, assuming a surface area of $A = 102$ m². The calculation requires the water content, which is presented in Figure 3c, to incorporate soil characteristics and computed hydraulic heads. The calculated results for soil salinity depicted in Figure 3d provide valuable insights into the areas in which the soil surface salinity may be higher and should be accounted for in regional soil remediation strategies. However, keep in mind that the results for soil salinity are only as accurate as the resolution of the available data for soil properties and distribution. In the next section, we utilize the evaluated model to demonstrate such effects by varying topsoil texture and structure.

3.2. Impact of soil texture and heterogeneity on salinity

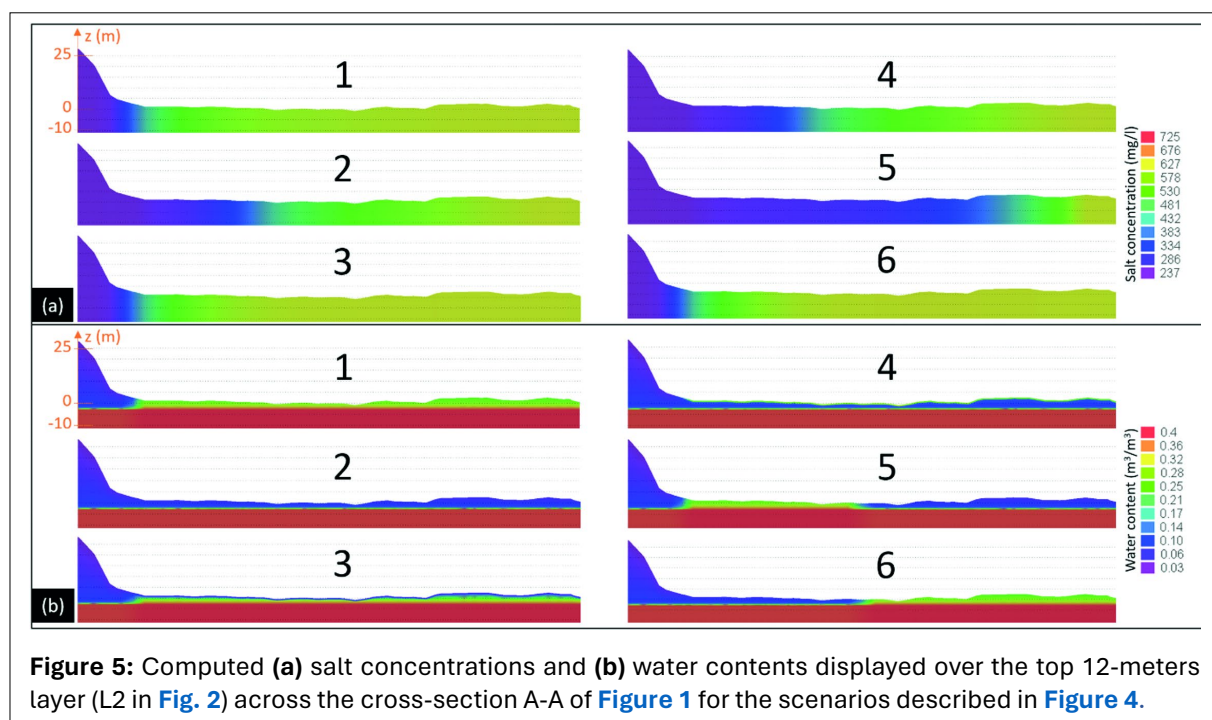
To evaluate the effect of soil texture and the presence of sharp textural contrasts on regional soil salinity driven by saltwater intrusion, we considered six hypothetical models that differed in soil texture and structure, as shown schematically in Figure 4. For each scenario, we used the geometric and morphological characteristics of the Altes Land region as the simulation domain. The soil textures and corresponding hydraulic characteristics are presented in Table 1. These scenarios were selected in order to investigate how (i) the soil texture (scenarios 1 and 2); (ii) the presence of a horizontal textural contrast by placing a thin (30 cm thick) layer of top soil overlying another layer that differed in texture (scenarios 3 and 4), and (iii) the presence of a vertical textural contrast located in the middle of the domain with equal distance to the river and hillslope (scenarios 5 and 6), influence soil salinity.

To specifically study the impact of soil texture and layering on soil salinity, we eliminated all external variables by assuming no evaporation and precipitation, except for the upward water gradient. This allowed us to examine the sole influence of soil properties on the process. To ensure consistency, we selected an equivalent saltwater head of $z = -3$ m for each side boundary. In this way, in contrast to Figure 3c, we maintained the entire surface of the domain above the groundwater level, resulting in uniform water content near the soil surface, which would mainly be affected by the properties of various soils. The salinity boundaries were identical to those used in the evaluated model. While the equivalent saltwater hydraulic head remained constant, varying salt concentrations on the boundaries generated

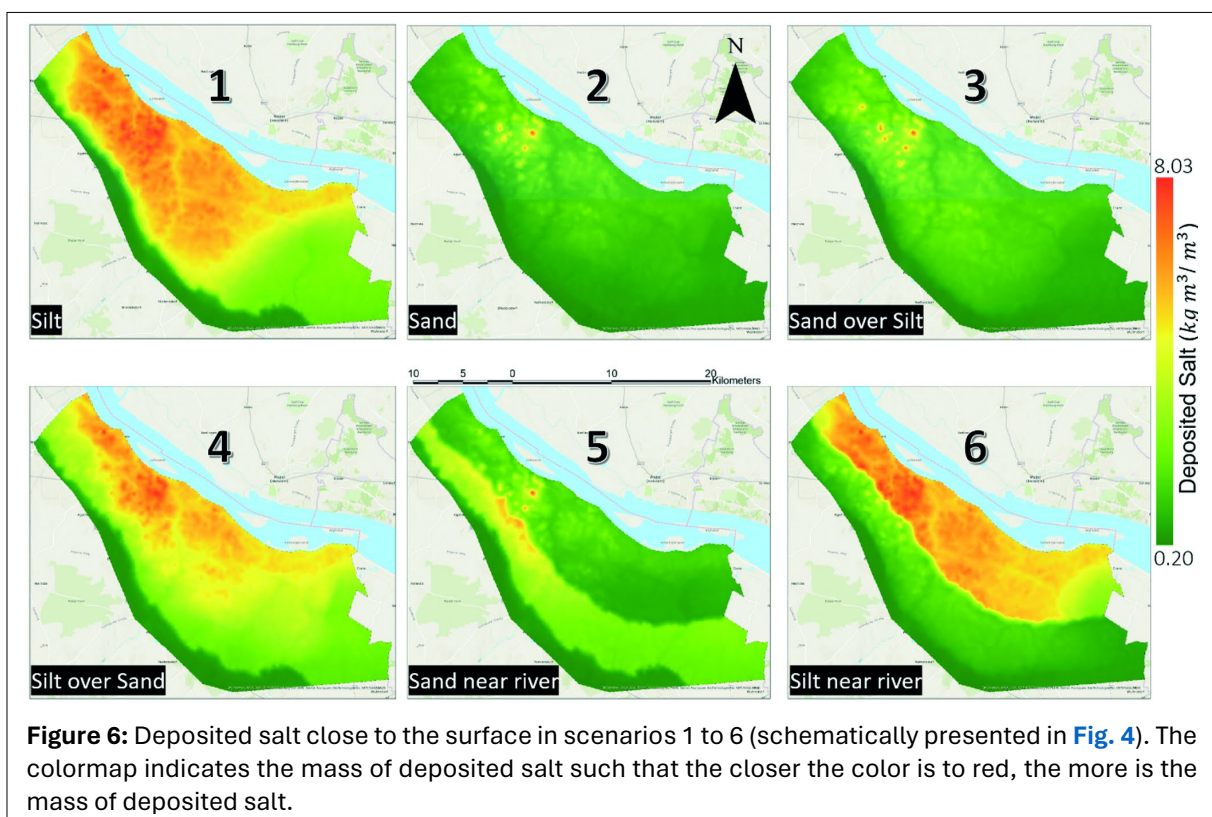


distinct hydraulic heads, thus establishing a relatively weak hydraulic gradient within the domain. In **Figure 5**, we present the computed salt concentrations and water contents along the cross-section A-A (depicted in **Fig. 1**), as well as for the top layer L2 (**Fig. 2**), under the scenarios illustrated in **Figure 4**. The computed results in this figure are essential for the calculation of surface soil salinity.

As shown in **Figure 5a**, altering the soil properties of the top layer influenced the lateral distribution of saline water. Specifically, when the top layer primarily consists of silt (as in scenarios 1 and 3), the salinity that originates from the riverside (right side of the model) infiltrates farther inland, when compared with the cases in which the top layer is predominantly composed of sand (scenarios 2 and 4). This suggests that compared to sand, silt serves as a more effective medium for the lateral propagation of salinity in unsaturated soil. Consequently, upon analyzing scenario 5, we observe that when the sand layer is adjacent to the right side (the riverside with higher salinity), it facilitates reduced lateral transport of the high-salinity water while allowing the propagation of salinity from the silt layer next to the hilly side, which exhibits a stronger capacity for transporting saline water. Consequently, the lateral propagation of saline water in this scenario is even lower than that in scenario 2, which features only a sand layer.



In **Figure 5a**, the displayed salt concentrations primarily reflect those of salt in the water within the pore space of the relatively saturated soil. However, it is important to keep in mind that actual soil salinity is influenced by topsoil water content. When the water content is higher in a particular soil type, the corresponding amount of salt with the same concentration in that area will also be higher. To accurately determine the salinity levels on the soil surface, it was necessary to consider the simulated water content, as depicted in **Figure 5b**. It is evident in this figure that there exists a region below the $z = -3$ m line that is fully saturated (red), exhibiting a water content of up to 0.4. The phenomenon of upward capillary transport through the soil was observed above this boundary, extending towards the soil surface. This behavior provides insights into the influence of soil texture and structure on the water-holding capacity and, ultimately, the actual amount of salt present on the soil surface. It can also be seen that in all scenarios, the water content in the vadose zone in the presence of silt is relatively higher than that in sand, which will in turn have a considerable impact on the soil salinity, calculated for all the scenarios via **Equation 3**, and is displayed in **Figure 6**. The results shown in **Figure 6** correspond to the surface soil salinity in an area of 102 m^2 with a thickness of 0.3 m.



According to **Figure 6**, owing to the low elevations (around $z = -3$ m) in several areas near the river in the northwest of the model domain (as reflected in the patches of regions with high salinity), the soil surface is saturated with groundwater, resulting in high salt accumulation. In other regions, the effects of soil texture and layering on the surface salt deposition were more pronounced. This suggests the importance of capillary liquid transport throughout the unsaturated zone, which connects the groundwater to the surface, on the surface soil moisture and salt concentration, and thus the total salt accumulation. Comparing scenarios 1 and 2, we observe that, compared to sand, there is more salt deposition close to the surface when the top layer is composed of silt. A comparison between the results for scenarios 1 and 3 indicates how the presence of a thin layer (30 cm thick) of sand over silt (scenario 3) drastically reduces salt deposition close to the soil surface. The presence of a thin layer of silt over sand however leads to significantly more salt deposition close to the surface when compared to the case in which the domain is composed of only sand (scenario 2). Regarding the effect of the uppermost soil layer, we compared two sets of scenarios: 1 and 4, and 2 and 3. These pairs shared identical soil properties in the top layer. Nevertheless, discernible differences in the deposition of salt were evident

when scenario pairs 1 and 4, as well as 2 and 3, were compared. Specifically, compared with scenarios 4 and 2, models 1 and 3 produced higher concentrations of salt on the soil surface. Comparing scenarios 5 and 6, it can be deduced that, in the presence of a vertical textural contrast, the order of layering plays a significant role in the amount of salt accumulated close to the surface. Note that the effective soil properties are the same in scenarios 5 and 6; however, the final field-scale response is completely different owing to the existence of local heterogeneity in the soil profile. The governing mechanisms controlling the observed differences in the six scenarios are discussed in the next section.

4. DISCUSSION

Based on the analysis of the results obtained under the various scenarios described in the previous section, we divided the influence of soil texture and structure on soil salinity into two categories:

- 1) Influence on soil surface water content
- 2) Impact on the propagation of salt concentration within the groundwater and vadose zones.

The interplay between the two gives rise to diverse patterns of salinity across the soil surface. To comprehensively analyze the impact of various mechanisms on soil salinity in diverse scenarios, we carried out a comparative study of the results described in the previous section. In what follows, we discuss each comparison, emphasizing the influence of individual mechanisms on the disparities observed in soil salinity levels.

4.1. Scenarios 1 & 2

The differences in soil salinity between the two media produced by the two scenarios depicted in [Figure 6](#) can be explained by variations in the water content on the soil surface and the propagation of salt concentration, as shown in [Figure 5](#). This figure indicates that the surface water content in the medium generated by scenario 1 (with silt) was higher than that in scenario 2 (with sand). This is consistent with the results of laboratory analyses conducted by others ([35](#), [36](#), [69](#)), where it was demonstrated that the length of the hydraulically connected paths throughout the unsaturated zone in silty media is larger than that in sandy ones. Therefore, a solute can be transported over longer distances above the groundwater that may even reach the soil surface.

In a medium according to scenario 1 (with surface water content $\theta > 0.25$), the presence of a positive lateral pressure gradient (from the river to the hilly side) allows for the transport of larger fluxes of salinity from the river side than in scenario 2 (with $\theta > 0.06$) where the water content is lower. In other words, silt, which has a higher unsaturated hydraulic conductivity under the same metric potential, exhibits a greater capacity for lateral flow than drier sand ([25](#), [41](#), [77](#)). This increased lateral flow in silt leads to a more extensive spread of salt concentration than in sand. Consequently, the combination of higher water content and salt concentration in scenario 1 ultimately led to a higher level of soil salinity than in the medium generated by scenario 2.

4.2. Scenarios 1 & 3 and 2 & 4

The media generated according to the two sets of scenarios exhibited discernible differences in the top 30 cm of the soil compared with the underlying layers. Examining the two pairs of model media generated by the scenarios shown in [Figure 5](#), the spread of salt concentration is relatively consistent within each pair. As a result, the primary factor contributing to the observed variations in soil surface salinity, as depicted in [Figure 6](#), is the presence of a thin layer of sand overlying silt in scenario 3 and, conversely, a thin layer of silt overlying sand in scenario 4. Through the regulation of the surface water content, the existence of such a thin layer is sufficient to significantly alter the patterns of salt accumulation on the surface.

Pores in sand are larger than those in silt, implying that a smaller capillary pressure is required to empty them ([62](#), [80](#)). This disrupts liquid continuity between the surface and groundwater, leading to reduced

salt deposition near the surface in the medium generated by scenario 3 when compared with the homogeneous silty medium in scenario 1. Conversely, the opposite was true for scenarios 2 and 4.

These findings agree with the experimental data reported by Shokri et al. (70) who conducted laboratory experiments in order to demonstrate how the addition of coarse-textured materials on top of fine-textured sandy materials limits the hydraulic connection between the surface and a receding evaporation front. Our field-scale numerical analysis confirms that the same underlying principles governing laboratory-scale processes also exert significant influence on large-scale processes.

4.3. Scenarios 1 & 4 and 2 & 3

In contrast to the previously described scenarios, the uppermost soil layer (top 30 cm) remained consistent across these pairs of scenarios. Although the distinctions in soil salinity between these pairs, as depicted in [Figure 6](#), are not as clear-cut as in the aforementioned scenarios, a comparison between scenario pairs 1 and 4, as well as pairs 2 and 3, reveals significant variations in soil salinity. Specifically, the soil salinity in the model according to scenario 1 was higher than that in scenario 4, whereas scenario 3 produced a medium that exhibited higher soil salinity than in scenario 2. Examination of [Figure 5](#) also indicates that the water content on the soil surface is very similar in the media produced by these scenario pairs, with the differences being primarily attributable to the variations in the lateral propagation of salt concentrations, a mechanism that was discussed in the Section 3.1 ([Scenarios 1 & 2](#)).

4.4. Scenarios 5 & 6

The objective of the comparison in this case is to demonstrate the potential for misinterpretation that can arise from relying solely on the effective parameters of porous media when studying transport phenomena in such heterogeneous media. In the case of the soil models generated by scenarios 5 and 6, the effective parameters of the soil are similar, differing only in the arrangement of the vertical layers. However, when considering the accumulation of salt near the soil surface, large-scale responses exhibit significant differences, which can be attributed to the influence of the layering structure and their arrangement on the flow and transport processes that occur within the porous media (71). [Figure 5](#) makes it evident that both the lateral expansion of salt concentration and the water content contribute to the distinction in the soil salinities. The underlying reasons for such disparities are described in the Section 3.1 ([Scenarios 1 & 2](#)).

4.5. Scenarios 2 & 5

The apparent differences between the underlying mechanisms that govern salt transport in the two media generated by scenarios 2 and 5 are intriguing and worth investigating. In the medium generated by scenario 5, which is characterized by the presence of a sandy top layer adjacent to the river, the propagation of salt concentration is significantly lower than that in the medium in scenario 2, where the entire top layer consists of sand. As illustrated in [Figure 6](#), the silt layer in the medium constructed in scenario 5 contained a relatively higher water content, which contributed to an overall higher surface soil salinity, when compared with scenario 2. However, the propagation of the salt concentration from the riverside through the sand layer to the silt layer was delayed. The delay, coupled with the propensity of silt to retain a higher water content, resulted in a larger portion of the salt concentration in the silt layer contributed by the left hilly boundary. Despite its connection to the sandy layer, which exhibits a minimal influx of salt from the riverside, the silt layer retained this concentration. This phenomenon is due to the dominance of a negative vertical pressure gradient in the silt layer in scenario 5 over the weak lateral pressure gradient vesseled through the relatively drier sand layer (2, 22).

The complexity arising from diverse soil textures and arrangements leads to distinct patterns of salt propagation and water distribution within the topsoil, ultimately resulting in varying levels of surface soil salinity. Although speculative, these scenarios underscore the importance of the precise characterization of soil profiles, particularly in proximity to the Earth's surface, in determining surface-level soil salinity.

Geological data for the Altes Land were derived from extensive spatiotemporal measurements. Despite distinguishing topsoil properties from a handful of other properties, such data collection does not always provide information on local soil texture and structure. A detailed mapping of topsoil arrangement and heterogeneity can, however, be challenging because of natural processes such as soil erosion and human activities, such as soil modification for agricultural purposes. However, the agricultural significance of Altes Land and the considerable impact of soil texture and structure on soil quality (as reflected in [Fig. 6](#)) motivate the necessity of including local topsoil characterization campaigns, which could be helpful in devising effective regional remediation plans for mitigating surface soil salinity. Favorable conditions for Altes Land to sustain its status as an agricultural hotspot entail the presence of shallow groundwater within the root zone, which exhibits very low levels of salinity. To achieve this, an optimal soil structure can be established based on various hypothetical scenarios. Among these scenarios, scenario 5 was identified as the most suitable, because it included a substantial proportion of agricultural land with optimal water content, particularly in the silty portion, owing to the presence of groundwater. Moreover, the impact of river salinity on this area was minimized by the presence of a top sandy layer adjacent to the river. This configuration ensures maximum accessibility to groundwater while effectively mitigating the adverse effects of salinity on the soil. Although the effects of climatic, anthropogenic, and hydrogeological parameters are important and must be taken into account, in practical efforts to mitigate the effects of salinity, the thickness and composition of the sand layer may be adjusted to maximize agricultural production while minimizing the propagation of soil salinity from the river.

5. LIMITATIONS AND OUTLOOK

The purpose of this study was to highlight the significance of different soil textures, structures, layering, and arrangements. To study the effects of soil layering on groundwater-associated soil salinity, we assumed that the geological layers were parallel to each other. The gradual accumulation of layers in the Altes Land beneath stagnant surface water supports this assumption. To develop higher resolution models of flow and transport processes in the type of geomedia that we studied, one must obtain or develop an all-encompassing geological map of the region, which, although costly, both economically and computationally, may be necessary. In addition, there is a strong correlation between soil texture and groundwater levels, which are intertwined with irrigation and meteorological patterns that are highly sensitive to variations on a temporal scale. To fully understand how soil texture affects soil salinity, it is necessary to consider these effects as transient events that occur at daily, monthly, or seasonal scales. Finally, we assumed that the topsoil is nonreactive, which might be a limiting assumption if clayey soil is present.

6. SUMMARY & CONCLUSIONS

We utilized extensive numerical simulations to investigate transport of saline water throughout the unsaturated zone of soil toward its surface, driven by saltwater intrusion in coastal regions. The effects of soil texture and arrangement on soil salinization were quantified at a regional scale. This was accomplished by first evaluating the numerical model using field-scale data collected from the Altes Land region located in the northern part of Germany. The region was selected due to the importance its soil quality on a wide range of socioeconomic activities in the Altes Land, as well as the availability of data that offer an excellent opportunity for evaluating our numerical model against field measurements. The predictions of the model were in agreement with the data; thus, the validated model was used to quantify the effect of soil texture and structure on soil salinity by devising six distinct hypothetical scenarios regarding the structure and text of the soil. The simulation results revealed the important role of soil characteristics in the complex interaction between saline groundwater and salt accumulation close to the soil surface at a regional scale. Our findings highlight the need for high-resolution data as well as computational models for soil texture and structure across agricultural hotspots that are vulnerable to soil salinity.

KEY POINTS:

Soil texture, heterogeneity, and arrangement strongly influence soil salinity at the regional scale.

High-resolution soil characterization is essential for devising effective remediation strategies against soil salinization.

Pore-scale physics and mechanisms govern macro-scale soil responses observed at regional scales.

STATEMENTS AND DECLARATIONS

Supplementary Material

See [Appendix A](#) for information on the "Field Measurements", which can be found online with this paper [here](#).

Acknowledgements

Funding by the Umwelt Bundesamt (UBA) in Germany under project number FKZ 37 2148 2050 is greatly appreciated. Groundwater recharge data and geological information were provided by the Geological Survey of Lower-Saxony (LBEG), groundwater measurements were provided by the Lower Saxony State Agency for Water Management, Coastal Protection and Nature Conservation (NLWKN), and the Elbe River data were provided by the Elbe River basin community (FGG Elbe), all of which are greatly appreciated.

Author Contributions

Vahid Sobhi Gollo: Conceptualization, data curation, formal analysis, investigation, methodology, software, validation, visualization, writing – original draft, review, editing and revising. **Muhammad Sahimi:** writing – review, editing and revising. **Eva González:** resources, writing – review and editing. **Jörg Elbracht:** resources, writing – review and editing. **Mithra-Christin Hajati:** resources, data curation, writing – review, editing and revising. **Peter Fröhle:** writing – review and editing. **Nima Shokri:** conceptualization, supervision, formal analysis, methodology, acquiring funding, writing – review, editing and revising.

Conflicts of Interest

There are no conflicts of interest to declare for any of the authors, and Nima Shokri, as the Editor in Chief of this journal, was not involved in the review process of this paper.

Data, Code & Protocol Availability

Surface Water Data

The data for surface water (water level and salinity) used in this study are openly available from the FGG Elbe at: <https://www.elbe-datenportal.de/FisFggElbe/content/start/BesucherUnbekannt.action>.

The FGG Elbe website exclusively presents its content in the German language. Below, we provide a comprehensive procedural account of how to extract data from the aforementioned link.

1. Initiate the process by selecting the checkbox labelled "Nutzungsbedingungen" (translated as terms of use).
2. Subsequently, activate the "Datenabruf" (data retrieval) button.

To access pertinent **hydraulic head measurements**, activate the "**Hydrologie**" (hydrology) button.

3. A new interface will emerge, which provides one with the following options: "Gewässer" and "Wasserkörper" (water body), "Messtelle" (measurement point), and "Parametergruppe" (parameter group).
4. We obtained the data for points 7 (measurement point: Stadersand) and 15 (measurement point: Blankenese Unterfeuer) of [Figure 1a](#) using the following parameter groups/settings:

- a. Chosen parameter group is "Wasserstand" (water table).
- b. The subsequent parameter choice encompasses both high tide (Tidehochwasser) and low tide (Tideniedrigwasser) alternatives.
- c. "Messwertart" (measurement type) can be specified as "Tagesmittelwert" (daily average).
- d. The "Messvorgang" (measurement process) can be defined as "kontinuierliche Messungen" (continuous measurements).
- e. The temporal domain is established through "Jahr von .. bis" (year from... till), commencing from 1978 and extending to the latest available measurement.
- f. The geospatial verification of each measurement point can also be performed through the "Kartenansicht" (map view) located on the right-hand side.
- g. The subsequent phase involves obtaining hydraulic head data by activating the "Ergebnisabruf" (result retrieval) option and selecting the ".xls" format as the preferred "Ausgabeformat" (output format).

To acquire salinity measurements, the process begins anew from the earlier mentioned link.

5. After activating the "Datenabruf" button, the subsequent step entails selecting the "allgemeine Gewässergüte" (general water quality) button.
6. Within the ensuing interface, to access salinity data, one must opt for "Salzgehalt" (Salinity) from the drop-down menu titled "Parametergruppe".
7. In the subsequent drop-down menu titled "Parameter", the designation "elektrische Leitfähigkeit" (electric conductivity) is selected.
8. The methodological approach for acquiring salinity data closely parallels the one elucidated earlier for hydraulic head measurements, and for which we used the following settings in order to obtain the data for the following measurement points used in **Figure 1a**:
 - a. Measurement point 3: Mittelkirchen
 - b. Measurement point 6: Symphonie
 - c. Measurement point 8: Schwingemündung
 - d. Measurement point 9: Tonne 112
 - e. Measurement point 10: Lühesander Süderelbe
 - f. Measurement point 11: Tonne 117
 - g. Measurement point 12: Lühewisch
 - h. Measurement point 13: Kraftwerk Wedel
 - i. Measurement point 14: Wittenbergen

The listed surface water data used in this study can be found under: Sobhi Gollo, V., Sahimi, M., González, E., Hajati, M.-C., Elbracht, J., et al. (2024). Soil salinization due to saltwater intrusion in coastal regions: The role of soil characteristics and heterogeneity. *InterPore Journal*, 1(1). Zenodo [Dataset]. <https://doi.org/10.5281/zenodo.10842112>

Groundwater Table and Salinity Information

The data for groundwater table and salinity used in this study are available from NLWKN and can be acquired at <http://www.wasserdaten.niedersachsen.de/cadenza/>. This website is only available in German. In order to obtain this information, please do as follows:

1. Navigate to the "Themen" (topics) section and select the "Grundwasser" (groundwater) category from the provided drop-down menu.
2. Upon opening the ensuing drop-down menu, you will find the option "Grundwasserstände-Messwerte" (measurements of groundwater Table) for groundwater table data and "Grundwassergüte - Messwerte" (measurements of groundwater Quality) for groundwater salinity data.
3. Clicking on either link will initiate a new window interface wherein users can make selections. These selections include specifying the "Messstelle" (measurement location), "Messjahr" (measurement year), and "Parameter" (parameter).

4. Within the context of the groundwater table data window, designate "Tagesmittelwert" (daily average) as the preferred parameter.
5. For the groundwater salinity data window, opt for "elektrische Leitfähigkeit" (electric conductivity) as the chosen parameter.
6. For the scope of this study, data has been acquired for the following points, which are shown in **Figure 1a**:
 - a. Measurement point 1 - Estebuegge UE 140 FI
 - b. Measurement point 2 - Ladekop UE 139 FI
 - c. Measurement point 4 - Hollern I
 - d. Measurement point 5 - Steinkirchen UE 135 FI
 - e. Measurement point 16 - Neukloster UE 28 FI
 - f. Measurement point 17 - Dollern G 3
 - g. Measurement point 18 - Dollern UE 137 FI

The listed groundwater data used in this study can be found under: Sobhi Gollo, V., Sahimi, M., González, E., Hajati, M.-C., Elbracht, J., et al. (2024). Soil salinization due to saltwater intrusion in coastal regions: The role of soil characteristics and heterogeneity. *InterPore Journal*, 1(1). Zenodo [Dataset]. <https://doi.org/10.5281/zenodo.10842112>

Information on models used







- The geological layers and the groundwater recharge model used in this study are available from the LBEG, for which the data may be obtained at NIBIS® Kartenserver.
 - The geological layers and groundwater recharge used in this study can be found under:

Sobhi Gollo, V., Sahimi, M., González, E., Hajati, M.-C., Elbracht, J., et al. (2024). Soil salinization due to saltwater intrusion in coastal regions: The role of soil characteristics and heterogeneity. *InterPore Journal*, 1(1). Zenodo [Dataset]. <https://doi.org/10.5281/zenodo.10842112>
- The Digital Elevation Model (DEM) used in this study is openly available from MERIT DEM at http://hydro.iis.u-tokyo.ac.jp/~yamada/MERIT_DEM/index.html
 - The DEM model used in this study can be found under: Sobhi Gollo, V., Sahimi, M., González, E., Hajati, M.-C., Elbracht, J., et al. (2024). Soil salinization due to saltwater intrusion in coastal regions: The role of soil characteristics and heterogeneity. *InterPore Journal*, 1(1). Zenodo [Dataset]. <https://doi.org/10.5281/zenodo.10842112>
- Groundwater modelling setup and results for both the evaluated and scenario-based models can be found in:
 - Sobhi Gollo, V., Sahimi, M., González, E., Hajati, M.-C., Elbracht, J., et al. (2024). Soil salinization due to saltwater intrusion in coastal regions: The role of soil characteristics and heterogeneity. *InterPore Journal*, 1(1). Zenodo [Dataset]. <https://doi.org/10.5281/zenodo.10842112>
 - To open these files, the user requires access to FEFLOW groundwater model (version 7.5) and ArcGIS (version 10).

Funding Received

Funding was provided by the Umwelt Bundesamt (UBA) in Germany under project number FKZ 37 2148 2050.

ORCID IDs

Vahid Sobhi Gollo	 https://orcid.org/0000-0002-5970-2475
Muhammad Sahimi	 https://orcid.org/0000-0002-8009-542X
Eva González	 https://orcid.org/0000-0002-8088-1404
Mithra-Christin Hajati	 https://orcid.org/0000-0002-9732-0021
Jörg Elbracht	 https://orcid.org/0000-0002-2045-9180
Peter Fröhle	 https://orcid.org/0000-0002-3903-7973
Nima Shokri	 https://orcid.org/0000-0001-6799-4888

REFERENCES

1. Adekiya, A.O., Ejue, W.S., Olayanju, A., Dunsin, O., Aboyeji, C.M., et al. (2020). Different organic manure sources and NPK fertilizer on soil chemical properties, growth, yield and quality of okra. *Scientific Reports* 10, 16083. <https://doi.org/10.1038/s41598-020-73291-x>
2. Aley, T.J., Kirkland, S.L. (2012). Down but not straight down: significance of lateral flow in the vadose zone of karst terrains. *Carbonates Evaporites* 27, 193–198. <https://doi.org/10.1007/s13146-012-0106-5>
3. Balfagón, D., Zandalinas, S.I., Mittler, R., Gómez-Cadenas, A. (2020). High temperatures modify plant responses to abiotic stress conditions. *Physiologia Plantarum*, 170, 335–344. <https://doi.org/10.1111/ppl.13151>
4. Bilal, S., Shahzad, R., Imran, M., Jan, R., Kim, K.M., Lee, I.-J. (2020). Synergistic association of endophytic fungi enhances Glycine max L. resilience to combined abiotic stresses: Heavy metals, high temperature and drought stress. *Industrial Crops and Products*, 143, 111931. <https://doi.org/10.1016/j.indcrop.2019.111931>
5. Boll, T., von Haaren, C., von Ruschkowski, E. (2014). The Preference and Actual Use of Different Types of Rural Recreation Areas by Urban Dwellers—The Hamburg Case Study. *PLoS ONE*, 9, e108638. <https://doi.org/10.1371/journal.pone.0108638>
6. Chaturvedi, A.K., Bahuguna, R.N., Shah, D., Pal, M., Jagadish, S.V.K. (2017). High temperature stress during flowering and grain filling offsets beneficial impact of elevated CO₂ on assimilate partitioning and sink-strength in rice. *Scientific Reports*, 7, 8227. <https://doi.org/10.1038/s41598-017-07464-6>
7. Chen, S., Mao, X., Shukla, M.K. (2020). Evaluating the effects of layered soils on water flow, solute transport, and crop growth with a coupled agro-eco-hydrological model. *Journal of Soils and Sediments*, 20, 3442–3458. <https://doi.org/10.1007/s11368-020-02647-7>
8. Cui, H., Bai, J., Du, S., Wang, J., Keculah, G.N., et al. (2021). Interactive effects of groundwater level and salinity on soil respiration in coastal wetlands of a Chinese delta. *Environmental Pollution*, 286, 117400. <https://doi.org/10.1016/j.envpol.2021.117400>
9. Dashtian, H., Shokri, N., Sahimi, M. (2018). Pore-network model of evaporation-induced salt precipitation in porous media: The effect of correlations and heterogeneity. *Advances in Water Resources*, 112, 59–71. <https://doi.org/10.1016/j.advwatres.2017.12.004>
10. Depke, S.-C., Lück, C., Peters, J., Wellmer, L., Seidel, S. (2016). Creating tangible and intangible hospitality products with a sustainable value – The case of the Altes Land apples. *Research in Hospitality Management*, 6, 37–43. <https://doi.org/10.2989/RHM.2016.6.1.5.1293>
11. Diersch, H.-J.G. (2014). FEFLOW. Springer Berlin Heidelberg, Berlin, Heidelberg. <https://doi.org/10.1007/978-3-642-38739-5>
12. DIN Deutsches Institut für Normung e.V. (2008). DIN 4220:2008-11, Bodenkundliche Standortbeurteilung - Kennzeichnung, Klassifizierung und Ableitung von Bodenkennwerten (normative und nominale Skalierungen). Beuth Verlag GmbH. <https://doi.org/10.31030/1436635>
13. Ertl, G., Bug, J., Elbracht, Dr. J., Engel, N., Herrmann, F. (2019). Grundwasserneubildung von Niedersachsen und Bremen. Berechnungen mit dem Wasserhaushaltsmodell mGROWA18. LBEG - Landesamt für Bergbau, Energie und Geologie. ISSN: 1864-6891. https://doi.org/10.48476/GEOBER_36_2019
14. FAO and ITPS. (2015). Status of the World's Soil Resources (SWSR) – Main Report. Food and Agriculture Organization of the United Nations and Intergovernmental Technical Panel on Soils, Rome, Italy. ISBN: 978-92-5-109004-6. <https://www.fao.org/3/i5199e/i5199e.pdf>
15. Francke, H., Thorade, M. (2010). Density and viscosity of brine: An overview from a process engineers' perspective. *Geochemistry*, 70, 23–32. <https://doi.org/10.1016/j.chemer.2010.05.015>

16. Gehrt, E., Benne, I., Evertsbusch, S., Krüger, K., Langner, S. (2021). Erläuterung zur BK50 von Niedersachsen. LBEG - Landesamt für Bergbau, Energie und Geologie. ISSN: 1864-6891 https://doi.org/10.48476/GEOBER_40_2021
17. Gelhar, L.W., Collins, M.A. (1971). General Analysis of Longitudinal Dispersion in Non-uniform Flow. *Water Resources Research*, 7, 1511–1521. <https://doi.org/10.1029/WR007i006p01511>
18. Ghassemi, F., Jakeman, A.J., Nix, H.A. (1995). Salinization of Land and Water Resources: Human Causes, Extent, Management and Case Studies. CAB International, Wallingford. ISBN: 0851989063, 9780851989068.
19. Ghavam, M., 2021. Relationships of irrigation water and soil physical and chemical characteristics with yield, chemical composition and antimicrobial activity of Damask rose essential oil. *PLoS ONE*, 16, e0249363. <https://doi.org/10.1371/journal.pone.0249363>
20. Goswami, R.R., Clement, T.P. (2007). Laboratory-scale investigation of saltwater intrusion dynamics: Dynamics of Saltwater intrusion. *Water Resources Research*, 43. <https://doi.org/10.1029/2006WR005151>
21. Guan, Y., Bai, J., Wang, J., Wang, W., Wang, X., et al. (2021). Effects of groundwater tables and salinity levels on soil organic carbon and total nitrogen accumulation in coastal wetlands with different plant cover types in a Chinese estuary. *Ecological Indicators*, 121, 106969. <https://doi.org/10.1016/j.ecolind.2020.106969>
22. Harter, T., Hopmans, J.W. (2005). Role of vadose zone flow processes in regional scale hydrology: Review, opportunities and challenges. *Frontis*. <https://library.wur.nl/ojs/index.php/frontis/article/view/897>
23. Hassani, A., Azapagic, A., Shokri, N. (2020). Predicting Long-term Dynamics of Soil Salinity and Sodicity on a Global Scale. *PNAS*, 117(52), 33017–33027. <https://doi.org/10.1073/pnas.2013771117>
24. Hassani, A., Azapagic, A., Shokri, N. 2021. Global Predictions of Primary Soil Salinization Under Changing Climate in the 21st Century. *Nature Communications*, 12, 6663. <https://doi.org/10.1038/s41467-021-26907-3>
25. Hendrickx, J.M., Flury, M. (2001). Uniform and preferential flow mechanisms in the vadose zone. In: Conceptual Models of Flow and Transport in the Fractured Vadose Zone. Washington, DC: The National Academies Press, p. 149–187. <http://nap.nationalacademies.org/10102>
26. Herrmann, F. (2013). Zeitlich und räumlich hochaufgelöste flächendifferenzierte Simulation des Landschaftswasserhaushalts in Niedersachsen mit dem Model mGROWA. *Hydrologie und Wasserbewirtschaftung / BfG*, 57.2013, 5ISSN 1439. https://doi.org/10.5675/HYWA_2013,5_2
27. Holland, K.T., Elmore, P.A. (2008). A review of heterogeneous sediments in coastal environments. *Earth-Science Reviews*, 89, 116–134. <https://doi.org/10.1016/j.earscirev.2008.03.003>
28. Hopmans, J.W., Qureshi, A.S., Kisekka, I., Munns, R., Grattan, S.R., et al. (2021). Critical knowledge gaps and research priorities in global soil salinity. *Advances in Agronomy*, 169, 1–191. <https://doi.org/10.1016/bs.agron.2021.03.001>
29. Huang, J., Zhang, G., Zhang, Y., Guan, X., Wei, Y., Guo, R. (2020). Global desertification vulnerability to climate change and human activities. *Land Degradation & Development*, 31, 1380–1391. <https://doi.org/10.1002/ldr.3556>
30. Huang, Y.-M., Liu, D., An, S.-S. (2015). Effects of slope aspect on soil nitrogen and microbial properties in the Chinese Loess region. *CATENA*, 125, 135–145. <https://doi.org/10.1016/j.catena.2014.09.010>
31. Janszen, A., Moreau, J., Moscariello, A., Ehlers, J., Kröger, J. (2012). Time-transgressive tunnel-valley infill revealed by a three-dimensional sedimentary model, Hamburg, north-west Germany: Time-transgressive tunnel-valley infill. *Sedimentology*, 60, 693–719. <https://doi.org/10.1111/j.1365-3091.2012.01357.x>
32. Jiang, Y., Ye, Y., Guo, X. (2019). Spatiotemporal variation of soil heavy metals in farmland influenced by human activities in the Poyang Lake region, China. *CATENA* 176, 279–288. <https://doi.org/10.1016/j.catena.2019.01.028>
33. Huysmans, M., Dassargues, A. (2005). Review of the use of Péclet numbers to determine the relative importance of advection and diffusion in low permeability environments. *Hydrogeology Journal*, 13, 895–904. <https://doi.org/10.1007/s10040-004-0387-4>
34. Kemfert, C., Kremers, H. (2009). The Cost of Climate Change to the German Fruit Vegetation Sector. *DIW Berlin Discussion Paper No. 857*, <https://ssrn.com/abstract=1430965> or <https://doi.org/10.2139/ssrn.1430965>
35. Lehmann, P., Assouline, S., Or, D. (2008). Characteristic lengths affecting evaporative drying of porous media, *Physical Review E*, 77, 056309, <https://doi.org/10.1103/PhysRevE.77.056309>
36. Lehmann, P., Or, D. (2009). Evaporation and capillary coupling across vertical textural contrasts in porous media. *Physical Review E*, 80, 046318. <https://doi.org/10.1103/PhysRevE.80.046318>
37. Li, X., Shi, F. (2021). Effects of evolving salt precipitation on the evaporation and temperature of sandy soil with a fixed groundwater table. *Vadose Zone Journal*, 20, e20122. <https://doi.org/10.1002/vzj2.20122>
38. Liu, J., Zhang, W., Long, S., Zhao, C. (2021). Maintenance of Cell Wall Integrity under High Salinity. *International Journal of Molecular Sciences*, 22, 3260. <https://doi.org/10.3390/ijms22063260>
39. Maas, E.V. (1986). Salt Tolerance of Plants. *Applied Agricultural Research*, 1, 12–26.

40. Memoli, V., De Marco, A., Esposito, F., Panico, S.C., Barile, R., Maisto, G. (2019). Seasonality, altitude and human activities control soil quality in a national park surrounded by an urban area. *Geoderma*, 337, 1–10. <https://doi.org/10.1016/j.geoderma.2018.09.009>
41. Mertens, J., Madsen, H., Feyen, L., Jacques, D., Feyen, J. (2004). Including prior information in the estimation of effective soil parameters in unsaturated zone modelling. *Journal of Hydrology*, 294, 251–269. <https://doi.org/10.1016/j.jhydrol.2004.02.011>
42. Meyer, K.-D. (2017). Pleistozäne (elster- und saalezeitliche) glazilimnische Beckentone und -schluffe in Niedersachsen/NW-Deutschland. *E&G Quaternary Science Journal*, 66, 32–43. <https://doi.org/10.3285/eg.66.1.03>
43. Mohanavelu, A., Naganna, S.R., Al-Ansari, N. (2021). Irrigation Induced Salinity and Sodicty Hazards on Soil and Groundwater: An Overview of Its Causes, Impacts and Mitigation Strategies. *Agriculture*, 11, 983. <https://doi.org/10.3390/agriculture11100983>
44. Nabiollahi, K., Golmohamadi, F., Taghizadeh-Mehrjardi, R., Kerry, R., Davari, M. (2018). Assessing the effects of slope gradient and land use change on soil quality degradation through digital mapping of soil quality indices and soil loss rate. *Geoderma*, 318, 16–28. <https://doi.org/10.1016/j.geoderma.2017.12.024>
45. Narjary, B., Kumar, S., Meena, M.D., Kamra, S.K., Sharma, D.K. (2021). Effects of Shallow Saline Groundwater Table Depth and Evaporative Flux on Soil Salinity Dynamics using Hydrus-1D. *Agricultural Research*, 10, 105–115. <https://doi.org/10.1007/s40003-020-00484-1>
46. NIBIS® Kartenserver, 2021. Lockergesteinsmodelle (3D-Modell Elbe Weser Region). - Landesamt für Bergbau, Energie und Geologie (LBEG), Hannover, Germany. <https://www.lbeg.niedersachsen.de/kartenserver/nibis-kartenserver-72321.html> or <https://geoportal.geodaten.niedersachsen.de/harvest/srv/api/records/ba58e478-dd6f-44c7-836c-9e75ac82f01d>
47. Norouzi Rad, M., Shokri, N., Sahimi, M. (2013). Pore-scale dynamics of salt precipitation in drying porous media. *Physical Review E*, 88, 032404. <https://doi.org/10.1103/PhysRevE.88.032404>
48. Pascual, L.S., Segarra-Medina, C., Gómez-Cadenas, A., López-Climent, M.F., Vives-Peris, V., Zandalinas, S.I. (2022). Climate change-associated multifactorial stress combination: A present challenge for our ecosystems. *Journal of Plant Physiology*, 276, 153764. <https://doi.org/10.1016/j.jplph.2022.153764>
49. Perri, S., Molini, A., Hedin, L.O., Porporato, A. (2022). Contrasting effects of aridity and seasonality on global salinization. *Nature Geoscience*, 15, 375–381. <https://doi.org/10.1038/s41561-022-00931-4>
50. Prävälíe, R. (2021). Exploring the multiple land degradation pathways across the planet. *Earth-Science Reviews*, 220, 103689. <https://doi.org/10.1016/j.earscirev.2021.103689>
51. Rad, M.N., Shokri, N., Keshmiri, A., Withers, P.J. (2015). Effects of Grain and Pore Size on Salt Precipitation During Evaporation from Porous Media. *Transport in Porous Media*, 110, 281–294. <https://doi.org/10.1007/s11242-015-0515-8>
52. Randazzo, A., Asensio-Ramos, M., Melián, G.V., Venturi, S., Padrón, E., et al. (2020). Volatile organic compounds (VOCs) in solid waste landfill cover soil: Chemical and isotopic composition vs. degradation processes. *Science of The Total Environment*, 726, 138326. <https://doi.org/10.1016/j.scitotenv.2020.138326>
53. Rauthe, M., Steiner, H., Riediger, U., Mazurkiewicz, A., & Gratzki, A. (2013). A Central European precipitation climatology—Part I: Generation and validation of a high-resolution gridded daily data set (HYRAS). *Meteorologische Zeitschrift*, 22(3), 235–256. <https://doi.org/10.1127/0941-2948/2013/0436>
54. Razafimaharo, C., Krähenmann, S., Höpp, S., Rauthe, M., Deutschländer, T. (2020). New high-resolution gridded dataset of daily mean, minimum, and maximum temperature and relative humidity for Central Europe (HYRAS). *Theoretical and Applied Climatology*, 142, 1531–1553. <https://doi.org/10.1007/s00704-020-03388-w>
55. Richards, L.A. (1931). Capillary Conduction of Liquids Through Porous Mediums. *Journal of Applied Physics*, 1, 318–333. <https://doi.org/10.1063/1.1745010>
56. Richter, D. (1995). Ergebnisse methodischer Untersuchungen zur Korrektur des systematischen Meßfehlers des Hellmann-Niederschlagsmessers". Offenbach am Main 1995 *Selbstverlag des Deutschen Wetterdienstes*. <http://nbn-resolving.org/urn:nbn:de:101:1-201601274368>
57. Rillig, M.C., Lehmann, A., de Souza Machado, A.A., Yang, G. (2019). Microplastic effects on plants. *New Phytologist*, 223, 1066–1070. <https://doi.org/10.1111/nph.15794>
58. Rivero, R.M., Mestre, T.C., Mittler, R., Rubio, F., Garcia-Sanchez, F., Martinez, V. (2014). The combined effect of salinity and heat reveals a specific physiological, biochemical and molecular response in tomato plants: Stress combination in tomato plants. *Plant, Cell & Environment*, 37, 1059–1073. <https://doi.org/10.1111/pce.12199>
59. Rivero, R.M., Mittler, R., Blumwald, E., Zandalinas, S.I. (2022). Developing climate-resilient crops: improving plant tolerance to stress combination. *The Plant Journal*, 109, 373–389. <https://doi.org/10.1111/tpj.15483>
60. Rotzoll, K., Fletcher, C.H. (2013). Assessment of groundwater inundation as a consequence of sea-level rise. *Nature Climate Change*, 3, 477–481. <https://doi.org/10.1038/nclimate1725>

61. Sadeghi, M., Shokri, N., Jones, S.B. (2012). A novel analytical solution to steady-state evaporation from porous media. *Water Resources Research*, 48, W09516. <https://doi.org/10.1029/2012WR012060>
62. Sahimi, M. (2011). *Flow and Transport in Porous Media and Fractured Rock: From Classical Methods to Modern Approaches* (2nd ed). Wiley-VCH, Weinheim. Print ISBN:9783527404858. <https://doi.org/10.1002/9783527636693>
63. Saxton, K.E., Rawls, W.J., Romberger, J.S., Papendick, R.I. (1986). Estimating Generalized Soil-water Characteristics from Texture. *Soil Science Society of America Journal*, 50, 1031–1036. <https://doi.org/10.2136/sssaj1986.03615995005000040039x>
64. Schenk, H.J., Jackson, R.B. (2002). The global biogeography of roots. *Ecological Monographs*, 72, 311–328. <https://doi.org/10.2307/3100092>
65. Schmidt, H., Seitz, S., Hassel, E., Wolf, H. (2018). The density–salinity relation of standard seawater. *Ocean Science*, 14, 15–40. <https://doi.org/10.5194/os-14-15-2018>
66. Shaar-Moshe, L., Blumwald, E., Peleg, Z. (2017). Unique Physiological and Transcriptional Shifts under Combinations of Salinity, Drought, and Heat. *Plant Physiology*, 174, 421–434. <https://doi.org/10.1104/pp.17.00030>
67. Shah, S.H.H., Vervoort, R.W., Suweis, S., Guswa, A.J., Rinaldo, A., van der Zee, S.E.A.T.M. (2011). Stochastic modeling of salt accumulation in the root zone due to capillary flux from brackish groundwater. *Water Resources Research*, 47. <https://doi.org/10.1029/2010WR009790>
68. Shokri, N. (2014). Pore-scale dynamics of salt transport and distribution in drying porous media. *Physics of Fluids*, 26, 012106. <https://doi.org/10.1063/1.4861755>
69. Shokri, N. (2019). Comment on “Analytical Estimation Show Low Depth-Independent Water Loss Due to Vapor Flux from Deep Aquifers by John S. Selker (2017).” *Water Resources Research*, 55, 1730–1733. <https://doi.org/10.1029/2018WR023347>
70. Shokri, N., Lehmann, P., Or, D. (2010). Evaporation from layered porous media. *Journal of Geophysical Research*, 115, B06204. <https://doi.org/10.1029/2009JB006743>
71. Shokri, N., Or, D. (2013). Drying patterns of porous media containing wettability contrasts. *Journal of Colloid and Interface Science*, 391, 135–141. <https://doi.org/10.1016/j.jcis.2012.08.074>
72. Shokri, N., Salvucci, G.D. (2011). Evaporation from Porous Media in the Presence of a Water Table. *Vadose Zone Journal*, 10, 1309–1318. <https://doi.org/10.2136/vzj2011.0027>
73. Shokri-Kuehni, S.M.S., Raaijmakers, B., Kurz, T., Or, D., Helmig, R., Shokri, N. (2020). Water Table Depth and Soil Salinization: From Pore-Scale Processes to Field-Scale Responses. *Water Resources Research*, 56. <https://doi.org/10.1029/2019WR026707>
74. Sobhi Gollo, V., Sahimi, M., González, E., Hajati, M.-C., Elbracht, J., et al. (2024). Soil salinization due to saltwater intrusion in coastal regions: The role of soil characteristics and heterogeneity. *InterPore Journal*, 1(1). Zenodo [Dataset]. <https://doi.org/10.5281/zenodo.10842112>
75. Steinmetz, D., Winsemann, J., Brandes, C., Siemon, B., Ullmann, A., et al. (2015). Towards an improved geological interpretation of airborne electromagnetic data: a case study from the Cuxhaven tunnel valley and its Neogene host sediments (northwest Germany). *Netherlands Journal of Geosciences*, 94, 201–227. <https://doi.org/10.1017/njg.2014.39>
76. van Genuchten, M.Th. (1980). A Closed-form Equation for Predicting the Hydraulic Conductivity of Unsaturated Soils. *Soil Science Society of America Journal*, 44, 892–898. <https://doi.org/10.2136/sssaj1980.03615995004400050002x>
77. Vereecken, H., Huisman, J.A., Bogena, H., Vanderborght, J., Vrugt, J.A., Hopmans, J.W. (2008). On the value of soil moisture measurements in vadose zone hydrology: A review. *Water Resources Research*, 44. <https://doi.org/10.1029/2008WR006829>
78. Wei, J., Zhou, J., Tian, J., He, X., Tang, K. (2006). Decoupling soil erosion and human activities on the Chinese Loess Plateau in the 20th century. *CATENA*, 68, 10–15. <https://doi.org/10.1016/j.catena.2006.04.011>
79. Werner, A.D., Ward, J.D., Morgan, L.K., Simmons, C.T., Robinson, N.I., Teubner, M.D. (2012). Vulnerability Indicators of Sea Water Intrusion. *Ground Water*, 50, 48–58. <https://doi.org/10.1111/j.1745-6584.2011.00817.x>
80. Wu, S., Gray, D.H., Richart, F.E. (1984). Capillary Effects on Dynamic Modulus of Sands and Silts. *Journal of Geotechnical Engineering*, 110, 1188–1203. [https://doi.org/10.1061/\(ASCE\)0733-9410\(1984\)110:9\(1188\)](https://doi.org/10.1061/(ASCE)0733-9410(1984)110:9(1188))
81. Yamazaki, D., Ikeshima, D., Tawatari, R., Yamaguchi, T., O’Loughlin, F., et al. (2017). A high-accuracy map of global terrain elevations. *Geophysical Research Letters*, 44, 5844–5853. <https://doi.org/10.1002/2017GL072874>
82. Yin, X., Feng, Q., Li, Y., Deo, R.C., Liu, W., et al. (2022). An interplay of soil salinization and groundwater degradation threatening coexistence of oasis-desert ecosystems. *Science of The Total Environment*, 806, 150599. <https://doi.org/10.1016/j.scitotenv.2021.150599>

83. Zamrsky, D., Karssenberg, M.E., Cohen, K.M., Bierkens, M.F.P., Oude Essink, G.H.P. (2020). Geological Heterogeneity of Coastal Unconsolidated Groundwater Systems Worldwide and Its Influence on Offshore Fresh Groundwater Occurrence. *Frontiers in Earth Science*, 7, 339. <https://doi.org/10.3389/feart.2019.00339>
84. Zandalinas, S.I., Sengupta, S., Fritschi, F.B., Azad, R.K., Nechushtai, R., Mittler, R. (2021). The impact of multifactorial stress combination on plant growth and survival. *New Phytologist*, 230, 1034–1048. <https://doi.org/10.1111/nph.17232>
85. Zhai, T., Wang, J., Fang, Y., Qin, Y., Huang, L., Chen, Y. (2020). Assessing ecological risks caused by human activities in rapid urbanization coastal areas: Towards an integrated approach to determining key areas of terrestrial-oceanic ecosystems preservation and restoration. *Science of The Total Environment*, 708, 135153. <https://doi.org/10.1016/j.scitotenv.2019.135153>
86. Zhang, Q., Wang, C. (2020). Natural and Human Factors Affect the Distribution of Soil Heavy Metal Pollution: a Review. *Water, Air, & Soil Pollution*, 231, 350. <https://doi.org/10.1007/s11270-020-04728-2>
87. Zhou, X.-Y., Wang, X.-R. (2019). Impact of industrial activities on heavy metal contamination in soils in three major urban agglomerations of China. *Journal of Cleaner Production*, 230, 1–10. <https://doi.org/10.1016/j.jclepro.2019.05.098>